Original Article

JCBFM

Journal of Cerebral Blood Flow & Metabolism
2018, Vol. 38(7) 1227–1242

DOI: 10.1177/0271678X17712388
journals.sagepub.com/home/jcbfm
SAGE

Kinetic modelling of [^{11}C]PBR28 for 18 kDa translocator protein PET data: A validation study of vascular modelling in the brain using XBD173 and tissue analysis

Mattia Veronese[1], Tiago Reis Marques[2,3], Peter S Bloomfield[3], Gaia Rizzo[4], Nisha Singh[1], Deborah Jones[5], Erjon Agushi[6], Dominic Mosses[6], Alessandra Bertoldo[4,7], Oliver Howes[2,3], Federico Roncaroli[6,*] and Federico E Turkheimer[1,*]

Abstract

The 18 kDa translocator protein (TSPO) is a marker of microglia activation in the central nervous system and represents the main target of radiotracers for the in vivo quantification of neuroinflammation with positron emission tomography (PET). TSPO PET is methodologically challenging given the heterogeneous distribution of TSPO in blood and brain. Our previous studies with the TSPO tracers [^{11}C]PBR28 and [^{11}C]PK11195 demonstrated that a model accounting for TSPO binding to the endothelium improves the quantification of PET data. Here, we performed a validation of the kinetic model with the additional endothelial compartment through a displacement study. Seven subjects with schizophrenia, all high-affinity binders, underwent two [^{11}C]PBR28 PET scans before and after oral administration of 90 mg of the TSPO ligand XBD173. The addition of the endothelial component provided a signal compartmentalization much more consistent with the underlying biology, as only in this model, the blocking study produced the expected reduction in the tracer concentration of the specific tissue compartment, whereas the non-displaceable compartment remained unchanged. In addition, we also studied TSPO expression in vessels using 3D reconstructions of histological data of frontal lobe and cerebellum, demonstrating that TSPO positive vessels account for 30% of the vascular volume in cortical and white matter.

Keywords

TSPO, [^{11}C]PBR28, kinetic modelling, endothelium, XBD173, immunohistochemistry, 3D modelling

Received 17 October 2016; Revised 11 April 2017; Accepted 28 April 2017

Introduction

The translocator protein (TSPO) is a five transmembrane domain 18 kDa protein located in the outer mitochondrial membrane.[1] In the brain, the TSPO is upregulated by microglial cells and macrophages during the inflammatory response, and to a much lesser extent in reactive astrocytes.[2,3] The TSPO therefore represents an ideal target for positron emission tomography (PET) studies aimed at imaging neuroinflammation in vivo.[4,5]

[1]Department of Neuroimaging, IoPPN, King's College London, London, UK
[2]Department of Psychosis Studies, IoPPN, King's College London, London, UK
[3]Institute of Clinical Sciences, Imperial College London, London, UK
[4]Department of Information Engineering, Padova University, Padova, Italy
[5]Department of Cellular Pathology, Salford Royal Foundation Trust, Salford, UK
[6]Division of Neuroscience and Experimental Psychology, University of Manchester, UK
[7]Padua Neuroscience Center, University of Padova, Padova, Italy

*Federico E Turkheimer and Federico Roncaroli share the senior authorship.

Corresponding author:
Federico E Turkheimer, Centre for Neuroimaging Sciences, IoPPN, King's College London, P089, De Crespigny Park, Denmark Hill, London SE5 8AF, UK.
Email: federico.turkheimer@kcl.ac.uk

Quantification of TSPO with PET is challenging regardless of the probe used.[6,7] [^{11}C]PK11195 gives a poor signal-to-noise ratio,[6] while the use of second-generation TSPO tracers is limited by the single nucleotide polymorphism (rs6971) in the *TSPO* gene,[8] which affects their binding affinity.[9] All TSPO radiotracers can bind plasma proteins, platelets and monocytes to various extents and such binding can be altered in pathological conditions affecting the peripheral immune system, such as systemic inflammation.[10–15] For these tracers, free plasma fractions are generally very low (<5%) and difficult to measure,[7,16] a matter that complicates further the quantification of image data. The uneven distribution of TSPO in the normal brain and its changes that occur in pathological states represent another challenge for the quantification of binding and affect the use of reference region approaches. Successful methods using the grey matter signal of healthy controls as pseudo-reference region have been developed for [^{11}C]PK11195[17] but never replicated with other tracers.

The expression of TSPO in the endothelium and tunica media of brain vessels[17] contributes to the background signal observed with [^{11}C]PK11195 and second generation tracers and this TSPO fraction in vessels is reduced in aged brains due to fibrosis of the vessel walls.[18] The contribution of vascular TSPO to the total measurable PET signal is expected to be proportional to the affinity of the tracer, and hence the high-affinity second generation compounds are more likely to be affected by vascular TSPO binding than the lower affinity tracers such as [^{11}C]PK11195. We previously proposed a 2TCM-1K model[19] for the quantification of the second generation ligand [^{11}C]PBR28[20] to account for the endothelial component of TSPO. Compared to the standard 2-tissues compartmental model (2TCM), 2TMC-1K includes the tracer binding to TSPO in vessels by adding an additional compartment in parallel to those describing the tissue tracer activity.[19] When applied to [^{11}C]PBR28 brain PET data in healthy controls, the 2TCM-1K model provided a statistically superior description of the [^{11}C]PBR28 uptake, reducing inter-subject variability but preserving the sensitivity for the known changes in affinity displayed by the populations with varying rs6971 genotypes[19] (high affinity binders – HABs; medium affinity binders MAB. The low affinity binders – LABS – were not included in the study). In simulations, 2TMC-1K also showed higher sensitivity to TSPO tissue changes compared to standard 2TCM.[19] The distribution volume estimates calculated using the 2TCM-1K model were shown to be better correlated with the TSPO mRNA mappings of the Allen Brain Atlas than those of the standard 2TCM.[19] When used in a [^{11}C]PBR28 brain PET study of subjects with schizophrenia, the 2TCM-1K was able to reproduce the same regional findings of previous studies that used [^{11}C]PK11195.[7,21]

This study aims to complete the validation of the 2TCM-1K model by comparing its sensitivity to changes in TSPO density with the 2TCM model. 2TCM-1K and 2TCM models were applied to data from seven patients with schizophrenia investigated with [^{11}C]PBR28 PET before and after the administration of a pharmacological dose of the TSPO agonist XBD173. The expectation was that in the 2TCM-1K analysis, the pharmacological blockade would correctly translate to comparable changes in the volume of distribution of the compartment describing the ligand specifically bound to TSPO (tissue and endothelial) but minimum changes of the compartment associated with the free tracer and non-specifically bound tracer fraction (i.e. non-displaceable compartment). In the standard 2TCM, we expected that changes in the target TSPO would map unpredictably on both the free and the bound tracer compartment. The second aim of the study was to profile the effects of XBD173 on the concentration of [^{11}C]PBR28 in the free and bound blood components as well as its radiometabolites to assess more generally the possibility of accurate quantification of pharmacological interventions targeting the TSPO. Finally, we investigated the TSPO expression in cortical and white matter vessels in samples of normal frontal lobe and cerebellum using immunohistochemistry data reconstructed with both a two-dimensional and three-dimensional (3D) approach.

Materials and methods

Datasets

The data used in this work were part of a study aiming to investigate neuroinflammation in schizophrenia with [^{11}C]PBR28 PET imaging. The study was approved by the Hammersmith Research Ethics Committee and was conducted in accordance with the Declaration of Helsinki. Subjects were given a full description of the study before providing written consent.

Seven males (average age 46 ± 10 years) diagnosed with schizophrenia were recruited from SLAM NHS Trust (London) and included in the study. All patients met the DSM-V criteria determined by clinical interview and review of the medical records. At the moment of PET scanning, patients were under stabilized treatment, all taking standard antipsychotics. Compared to baseline scan, there was minimum change in antipsychotic medications in five patients out of seven. On those cases where a change on antipsychotic medication occurred, patients kept similar chlorpromazine equivalents. All the subjects were also tested for the rs6971 TSPO genetic

polymorphism and only homozygote high-affinity binders (HABs) were included in the analysis.

Experimental protocol

Each participant had two PET scans with [^{11}C]PBR28: the first at baseline conditions, and the second after XBD173 administration. The two [^{11}C]PBR28 PET scans were performed at different days: six out of the seven subjects, previously included in,[21] had the baseline PET scan approximately two years (866 ± 82 days) before the XBD173 scan. Only one subject had both baseline and blocked scan within a week of each other. Notably, PET scans started at a similar time of day (mean injection time: 14:32; earliest injection:10:46; latest injection: 15:56) to reduce intra- and inter-subject variability, limiting the effects of circadian rhythms on TSPO density.[22,23]

All the subjects underwent high-resolution T1 magnetic resonance imaging (MRI) in a Siemens Tim Trio 3T scanner (Siemens Healthcare, Erlangen, Germany). These structural MRI images were coregistered with the PET imaging to identify the anatomical regions of interest.

Administration of XBD173

XBD173 is a selective TSPO agonist developed for the treatment of generalized anxiety, and previously tested in occupancy studies.[24] All the subjects received an oral dose of 90 mg dose of XBD173, corresponding to 0.98 ± 0.16 mg/Kg (mean $\pm$ SD) normalized dose based on the patient weight. Assuming an effective dose of 0.34 mg/kg to reach 50% of target occupancy (ED50),[24] the administered dosage of XBD173 aimed to reach between 66% and 77% of TSPO brain occupancy. The timing of radiotracer injection was also designed to match the peak concentration of the drug in blood according to Owen et al.[24] No measure of XBD173 plasma concentration was taken during the study to control for individual differences in pharmacokinetics.

PET imaging

An initial low-dose computer tomography (CT) scan was acquired for attenuation and scatter correction using Siemens Biograph^{TM} True Point^{TM} PET/CT scanner (Siemens Medical Systems, Germany). Subjects then received a bolus injection of [^{11}C]PBR28 (target dose ~300 Mbq) followed by a 90-min PET emission scan. PET data were acquired in 3D mode and binned into 26 frames (durations: 8×15 s, 3×1 min, 5×2 min, 5×5 min, 5×10 min). Images were reconstructed using filtered back projection and corrected for attenuation and scatter. Radiopharmaceutical preparation of [^{11}C]PBR28 was done as described in Owen et al.[24] and it was consistent with previous studies.[21]

In parallel to the PET acquisition, arterial blood was sampled from the radial artery using a combined automatic and manual approach. A continuous sampling system (ABSS Allogg, Mariefred, Sweden) was used to measure whole blood activity for the first 15 min of each scan at the rate of one sample per second. Discrete blood samples were manually taken at 5, 10, 15, 20, 25, 30, 40, 50, 60, 70, 80, 90 min, centrifuged and used to determine the plasma over blood activity ratio (POB). Samples at 5, 10 and 15 min were used to calibrate the two sampling modalities. Samples taken at 5, 10, 20, 30, 50, 70 and 90 min were also analysed using HPLC to calculate the plasma fraction of tracer free of metabolites (PPf). Radiometabolite analysis of [^{11}C]PBR28 in the blood was done as described previously.[21,24]

Image analysis

Structural MRI images were used for grey/white matter segmentation and region of interest (ROI) definition. A neuroanatomical atlas was co-registered on each subject's MRI scan and PET image using a combination of Statistical Parametric Mapping 8 (http://www.fil.ion.ucl.ac.uk/spm) and FSL (http://www.fsl.fmrib.ox.ac.uk/fsl) functions, implemented in MIAKAT^{TM} (http://www.imanova.co.uk). ROIs included occipital lobe, temporal lobe, frontal lobe, parietal lobe, insular cortex, cingulate cortex, amygdala, hippocampus, thalamus, striatum and cerebellum.

All PET images were corrected for head movement using non-attenuation-corrected images as they include greater scalp signal, which improves re-alignment compared to attenuation-corrected images. Frames were realigned to a single ''reference'' space identified by the PET frame with the highest activity. The transformation parameters were then applied to the corresponding attenuation-corrected PET frames to create a movement-corrected dynamic image for analysis. Regional TACs were obtained by sampling the image with the co-registered atlas.

To investigate the effect of XBD173 on [^{11}C]PBR28 uptake, standardised uptake values (SUV), using injected dose and patient weight as normalisation factors, were computed 90 min after tracer injection for each PET scan.

Blood data processing

Processing of blood samples was performed consistently with previous studies.[21] Both POB and PPf were fitted with an extended Hill model[25] that provided the best data description.[26] Whole blood TACs were fitted using a variation of Feng's model that consists in a

straight line to the arterial input function peak followed by a tri-exponential decay.[27] For each scan, the difference between tracer arrival time in the brain and arterial sampling site was estimated by shifting blood curves 0–20 s (both parent and whole blood TACs), fitting the whole brain TAC (using exponential spectral analysis to avoid dependency on a particular compartmental model), and selecting the delay that produced the smallest weighted residual sum of squares.

Kinetic analysis

Quantification of [^{11}C]PBR28 tissue distribution was performed using both the 2TCM-1K and the standard 2TCM. Note that these kinetic models share most of the microparameters with the exception of K_b which is explicitly used in 2TCM-1K to account for the endothelial TSPO component.[19] A summary of the model configurations and kinetic parameters is reported in the supplementary material – Figure 1.

Both 2TCM-1K and 2TCM models were solved using the weighted nonlinear least square estimator (WNLLS), as implemented in Matlab2012b (The Mathworks Inc., Natick, MA). Initial microparameter values were set based on the literature[19], while weights for the individual data points were defined as the inverse of the variance of the PET measurement error. This was assumed to be additive, uncorrelated, normally distributed with a zero mean and variance equal to the decay-corrected activity divided by the length of the relative scan interval, multiplied by a scale factor, estimated a posteriori.[28] The total distribution volume (V_T) was then determined (regions with V_T estimates higher than 10 mL/cm^3 or with unreliable precision (CV > 50%) were excluded from the analysis as non-physiological based on previous analysis[19]). For both models, the blood volume fraction (V_b) was estimated together with the other model microparameters.

The comparison between the two models was done first by assessing fit performance and data model description efficiency as measured by the Akaike information criterion (AIC).[29] The two models were then assessed in term of total signal compartmentalisation: changes of total distribution volume (V_T) before and after blocking were correlated with the changes of specific binding (as indicated by k_3/k_4) and non-displaceable binding (as indicated by K_1/k_2 ratio). For 2TCM-1K, the endothelial binding changes (ΔK_b) were also calculated and compared to changes in the tracer specific binding (k_3/k_4).

Statistical analysis

Statistical analysis was conducted in SPSS version 21 (www.spss.com). Two-tailed paired *t*-tests were used to assess whether there were statistically significant differences between [^{11}C]PBR28 PET scans at baseline and after XBD173 blockage. Target variables of this analysis included experimental settings and tracer dosing, blood and tissue tracer uptakes, as well as compartmental modelling kinetic estimates. The Pearson's linear correlation coefficient was used to test for the presence of any association between [^{11}C]PBR28 plasma free fraction and [^{11}C]PBR28 tissue kinetics.

Variation of V_T estimates (before and after blocking) for both 2TCM and 2TCM-1K was correlated with the TSPO mRNA expression mappings contained in the Allen Human Brain Atlas (http://www.brain-map.org).[30] We have previously shown that these maps are highly predictive of protein levels in-vivo measured with PET for all those transcripts that do not undergo significant post-transcriptional modifications.[31] We hypothesised that the reduction of [^{11}C]PBR28 binding due to XBD173 TSPO blocking would be proportional to the TSPO mRNA expression. Changes for SUV, K_1/k_2 and k_3/k_4 were also considered. Processing and analysis of mRNA data were run using the software application MENGA.[32]

Assessment of vascular TSPO in normal human brain

The anterior superior frontal lobe and the cerebellum of three normal brains were obtained from the Multiple Sclerosis and Parkinson's Disease Tissue bank at Imperial College, UK. For each case, 10 μm thick sections were cut from formalin fixed paraffin embedded (FFPE) tissue blocks. Immunostains were performed using immunoperoxidase and immunofluorescence with antibodies directed against the vascular marker CD31, the glial fibrillary acidic protein (GFAP) and TSPO. The sections were deparaffinised by heating for 20 min in an oven at 60°C, 3 × 10 min in 100% xylene, 2 × 5 min in 100 ethanol, 5 min in 90% ethanol, 5 min in 70% ethanol and 2 × 5 min in water. For immunoperoxidase, the sections were immersed for 20 min in steam-heated sodium citrate buffer (10 mM sodium citrate, 0.05% v/v Tween 20, pH 6) followed by quenching of endogenous peroxidase in methanol and 1% v/v hydrogen peroxide for 15 min. The sections were thereafter incubated with the primary antibody at the following dilutions: CD31 (Dako Clone JC7QA Ref M0823 (1:30), anti-GFAP (Dako Clone 6F2 Ref M0761, dilution 1:200) and anti-TSPO (Abnova, goat polyclonal; dilution 1:500). The SuperSentitive IHC detection system from BioGenex (Fremon, CA, USA) was used the next day for visualisation as per the manufacturer's instructions. Finally, sections were counterstained with Mayer's Haemalum before being dehydrated and cover slipped.

The specificity of the anti-TSPO antibody was tested. Immunoreactions with omission of the primary

antibody were performed as negative controls and sections of adrenal cortex were included in each batch as positive controls. The epitope recognised by the anti-TSPO antibody corresponds to amino acids 158–169, which are unique to human TSPO (Blast/Fasta; www.pir.georgetown.edu). A Western-blot was also run with total protein extracts from human normal adrenal glands that constitutively contain high level of TSPO. Results are shown in supplementary material – Figure 2.

Double immunofluorescence with CD31/TSPO and GFAP/TSPO was carried out as follows. A cocktail of both antibodies in donkey serum buffer (PBS + 0.5% v/v donkey serum, 1% w/v BSA and 0.01% w/v sodium azide) was applied onto sections and incubated overnight at room temperature. CD31 and GFAP were detected with the donkey anti-mouse Alexa Fluor 488 (Life Technologies, Warrington, UK) and TSPO was detected with secondary biotinylated anti-goat antibodies (Vector Labs, Burlingame, CA, USA) and a complex of biotin and streptavidin conjugated Alexa Fluor 546 (Life technologies). Secondary antibodies were incubated for 45 min and the avidin-biotin complex for 1 h. Sections were then incubated with DAPI (Life Technologies) in PBS for 30 min, rinsed three times and coverslipped using mountant for fluorescence microscopy (DAKO). Images were ascertained by fluorescent microscopy using the LEICA TCS SP5 II confocal microscope with integrated application suite (Version: 2.5.2.6939; Leica Microsystems GmbH, Wetzlar, Germany).

3D reconstructions of cortical and white matter vessels and 3D analysis of vascular TSPO were performed using a method previously described.[33] Full details of the procedure are reported in the supplementary materials.

Distribution analysis of the TSPO and the ubiquitous CD31 was also performed using the Bitplane Imaris 3D/4D imaging software (Bitplane AG Zurich, Switzerland). 3D images were cropped using the crop 3D tool to form a 500 μm^3 section. For effective analysis of stained volume in Imaris, the voxel size of the 3D image must be consistent with that of the original scanned slides. To achieve this, measurements were made upon the slides' localised viewpoints in Caseviewer and an x and y value obtained by dividing Caseviewer's horizontal and vertical image size values by the number of pixels; identified by ImageJ. Z values were obtained using the thickness of each original tissue slice, in this case 6 μm. TSPO expression was calculated by carefully overlaying the TSPO staining with CD31 in order to select only vascular TSPO rather than tissue microglia. Perivascular macrophages were too close to the vessel walls to be excluded from quantification. In this respect, the TSPO volumes in vessels were slightly overestimated.

Identification of the TSPO and CD31 stained surfaces was refined in Imaris using background thresholding once images were cropped to the three distinct 500 μm^3 ROI. While background intensity of the images had been adjusted previously, the Imaris surface editing tool requires adjustment once again at this point at the discretion of the data analyser. Once surfaces were identified, the Imaris vantage tool was used to attain values of the two stained surfaces such that ROI volumes ratios between the TSPO and CD31 stacks were conserved. Results were analysed with a one-way ANOVA with Dunnett's post hoc tests, performed using GraphPad Prism version 5.00 for Windows (GraphPad Software, San Diego California USA, www.graphpad.com).

Results

Tracer dosing and experimental variables

We observed no difference in the injected doses between baseline scans (mean ± SD: 321 ± 32 MBq) and blocking scans (mean ± SD: 302 ± 75 MBq). In contrast, injected mass (BASELINE mean ± SD: 2.2 ± 0.6 μg; BLOCKING mean ± SD: 4.1 ± 2.1 μg) and specific activity (BASELINE mean ± SD: 53.7 ± 13.7 GBq/μmol; BLOCKING mean ± SD: 32.7 ± 14.6 GBq/μmol) were significantly different between conditions. Analyses refer to two-tailed paired t-tests, with the p-value = 0.05 set as the threshold for significance.

Motion statistics were comparable between conditions (total motion *baseline* = 15.5 ± 7.1 mm; total motion follow-up = 12.4 ± 3.9 mm; two-tailed paired t-test p-value = 0.42) and consistent with an age-matched independent dataset of [^{11}C]PBR28 brain PET scans of healthy volunteers[21] (total motion *healthy controls* = 14.6 ± 4.4 mm; two-samples t-test p-value = 0.27).

Blood data analysis

Arterial whole blood and plasma activities were significantly affected by XBD173 administration, compared to baseline conditions (Figure 1). Peak activities and area under the curve (AUC) for both plasma (Cp) and whole blood (Cb) TACs significantly increased in the second scan, with mean ± SD relative differences of 84 ± 79% for peak Cp, 30% ± 33% for peak Cb, 58% ± 29% for AUC Cp, and 58% ± 29% for AUC Cb. These variations are consistent with the reduction of tracer target availability throughout the body, following TSPO blockage by XBD173.

Plasma-over-blood ratios and parent plasma fractions also changed with XBD173 blocking (Figure 2). There was a statistically significant group effect

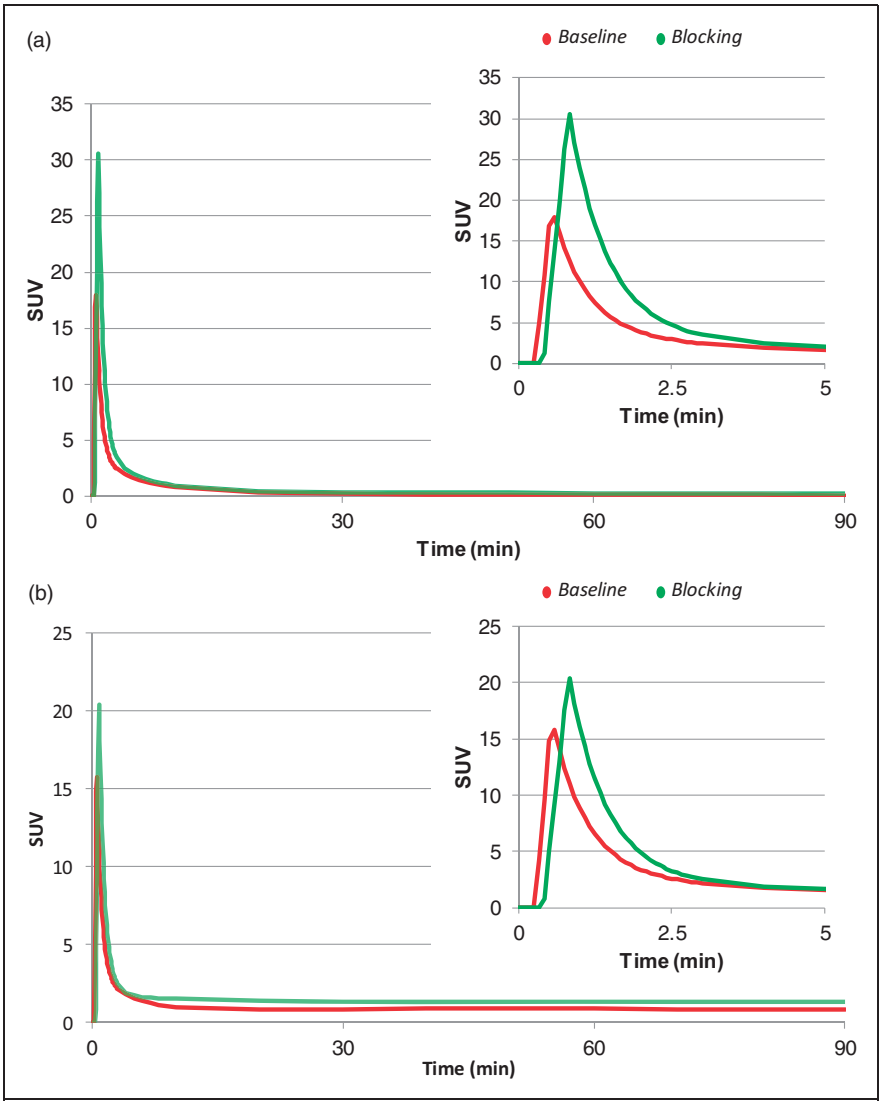

Figure 1. Effect of XBD173 on [^{11}C]PBR28 arterial input functions. [^{11}C]PBR28 kinetics in arterial parent plasma (a) and whole blood (b) are reported for a representative subject with schizophrenia. For each panel full kinetics (0–90 min) and TAC peaks (0–5 min) are shown. Red lines refer to baseline. Green lines refer to TSPO blocking with 90 mg of XBD173.

in the repeated-measure ANOVA for both POB (p-value = 0.005) and PPf (p-value = 0.006), supporting the impact of the blocking agent XBD173 on the plasma-blood tracer interaction as well as on [^{11}C]PBR28 radiometabolite kinetics. The increased POB in the initial phase ($\Delta POB_{10\text{-}30\,min}$ = 35%% ± 25%) as well as the reduced parent fraction in the XBD173 ($\Delta PPf_{10\text{-}30\,min} = -34\%\% \pm 17\%$) likely indicated the higher plasma availability of the tracer, given that the TSPO fraction on platelets and red cells was reduced by the blocking agent; hence more parent was amenable to metabolism and the parent fraction degraded more quickly.

Free plasma fractions (f_p) showed a high variability between scans (mean ± SD relative difference: 6% ± 40%, min variation −19%, max variation +81%), although these differences were not significant (two-tailed paired t-test, p-value > 0.05).

[^{11}C]PBR brain PET uptake

The administration of XBD173 led to a generalised reduction of [^{11}C]PBR28 PET uptake across the entire brain in all subjects. SUV analysis showed mean ± SD relative changes of −40% ± 7% for whole brain, and −44% ± 8% for cortical grey matter. No region was excluded by tracer uptake displacement, including cerebellum (SUV relative difference −47%% ± 8%, mean ± SD) (Supplementary material – Figure 3). These reductions remained

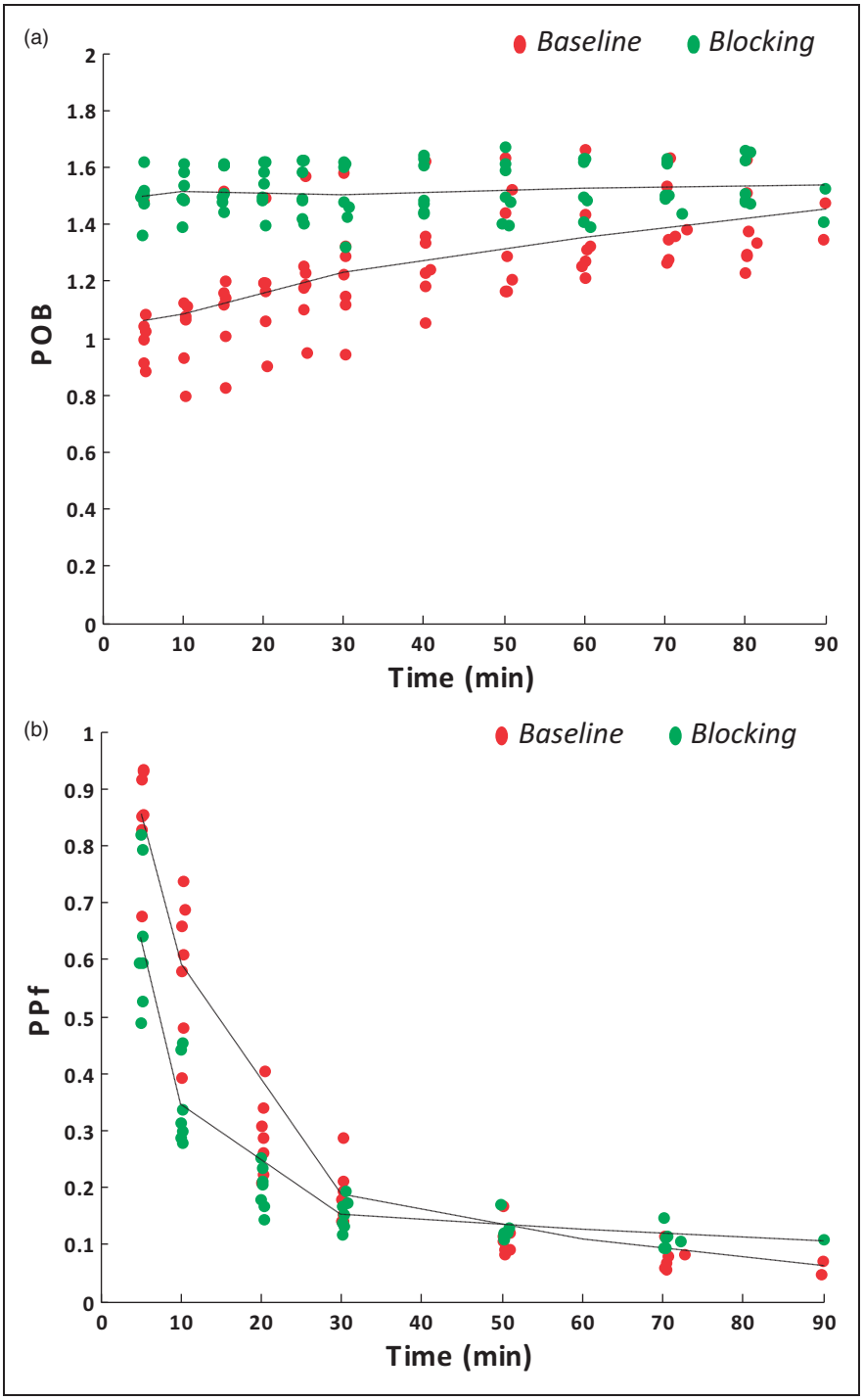

Figure 2. Effect of XBD173 on [^{11}C]PBR28blood metabolism. [^{11}C]PBR28 plasma-over-blood ratio (POB) and parent plasma fraction (PPf) are reported for a representative subject with schizophrenia (panels A and B, respectively). Red samples refer to baseline. Green samples refer to TSPO blocking with 90 mg of XBD173.

significant even when the tracer specific activity was used as a covariate in the analysis (ANOVA, p-value = 0.02), with no interaction between specific activity and SUV (p-value = 0.97).

[^{11}C]PBR PET kinetic analysis

Comparison of model performances. The analysis of the statistical performance of the kinetic models confirmed

2TCM-1K to be superior to 2TCM for the description of [^{11}C]PBR28 data after XBD173 blocking at the regional level. This finding is consistent with the previous applications of [^{11}C]PBR28 in healthy and pathological populations.[19,21] The 2TCM-1K provided a better fit of the tissue data in 83% of the analysed ROIs (Figure 3). Note that the regions for which 2TCM outperformed 2TCM-1K were all concentrated in a unique subject, for which we noted different [^{11}C]PBR28 kinetics compared to the other subjects (Supplementary material – Figure 4). The relative difference of the weighted residual sum of squares obtained with 2TCM-1K, compared to the 2TCM one, was $-39\% \pm 23\%$ (mean $\pm$ SD). Weighted residuals obtained with 2TCM-1K were consistent with the assumptions on the measurement error (random and uncorrelated) but not those obtained with the 2TCM.

In terms of parsimony criteria, the AIC for the 2TCM-1K AIC model was smaller than 2TCM AIC in 75.1% of the regions where both models successfully converged to a physiological solution, thus confirming the identification of 2TCM-1K as the optimal model to describe [^{11}C]PBR28 brain data (Supplementary Material – Table 1).

In term of outliers, the two models performed similarly (brain outlier fraction: 12% for 2TCM and 10% for 2TMC-1K). These were concentrated particularly in small regions (average volume $<3\,cm^3$) necessarily characterized by high noise data. After correction for outliers, individual V_T estimate precisions were consistent for both models: for 2TCM CV Repetition $=9\% \pm 9\%$; for 2TCM-1K CV $V_T = 8\% \pm 7\%$.

Kinetic estimates. The results of [^{11}C]PBR28 PET data quantification using 2TCM-1K and 2TCM models are

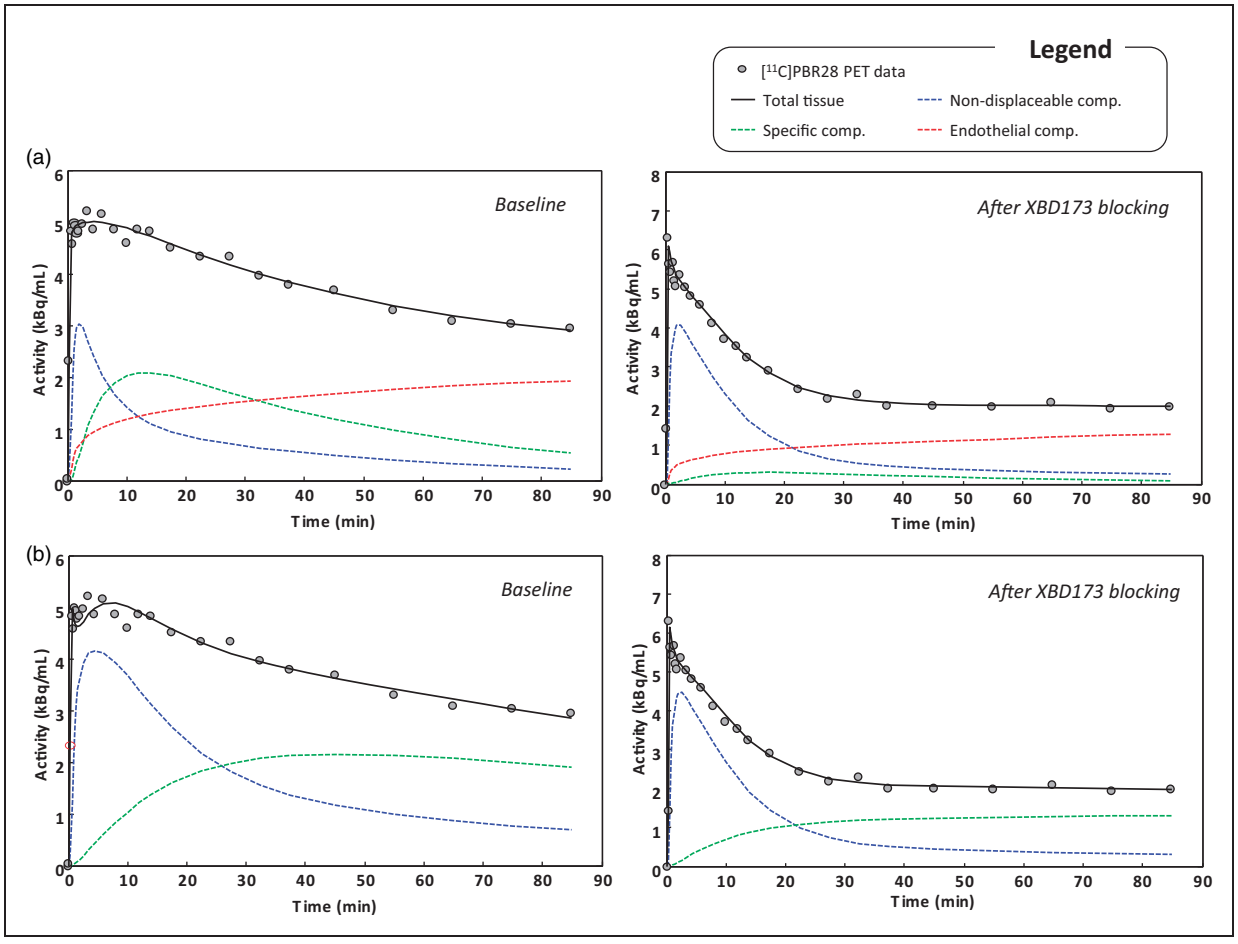

Figure 3. [^{11}C]PBR28 brain PET data fit and model compartmentalisation. Example of model fits to whole brain activity with 2TCM-1K (a) and standard 2TCM (b). Data belong to a representative subject with schizophrenia, investigated at baseline conditions and after XBD173 blocking. For each panel, black circles represent measured activity curve while solid black lines represent the model description. Single compartmental kinetics are also reported with blue, green and red lines representing non-displaceable, specific and endothelial binding, respectively.

reported in Supplementary Material – Table 2 and 3, respectively. In 2TCM-1K, mean parameter estimates for V_T and k_3/k_4 reduced from baseline to blocking in all the ROIs ($-60\% \pm 24\%$ for V_T; $-71\% \pm 23\%$ for k_3/k_4) (Figure 4(a)). The non-displaceable component K_1/k_2, instead, showed lesser variations ($-14\% \pm 48\%$) and even slightly increased in some ROIs like amygdala and thalamus (Figure 4(a)). Changes of the endothelial bound fraction were also consistent with the administration of TSPO blocking agent, with a mean reduction ranging between 48% and 65% (Supplementary material - Table 4). In term of absolute values, the highest changes were detected in the specific compartment (k_3/k_4 mrd%: -86% to -26%). These values were highly correlated with V_T changes (Pearson's $r = 0.85$). In contrast, the lowest changes were detected in the non-displaceable compartment (K_1/k_2 mrd%: -21% to $+15\%$).

In the case of the 2TCM, the parameter estimates for V_T, K_1/k_2 and k_3/k_4 were reduced after XBD173 administration but the relative relationship was different compared to 2TCM-1K (Figure 4(b)). The highest

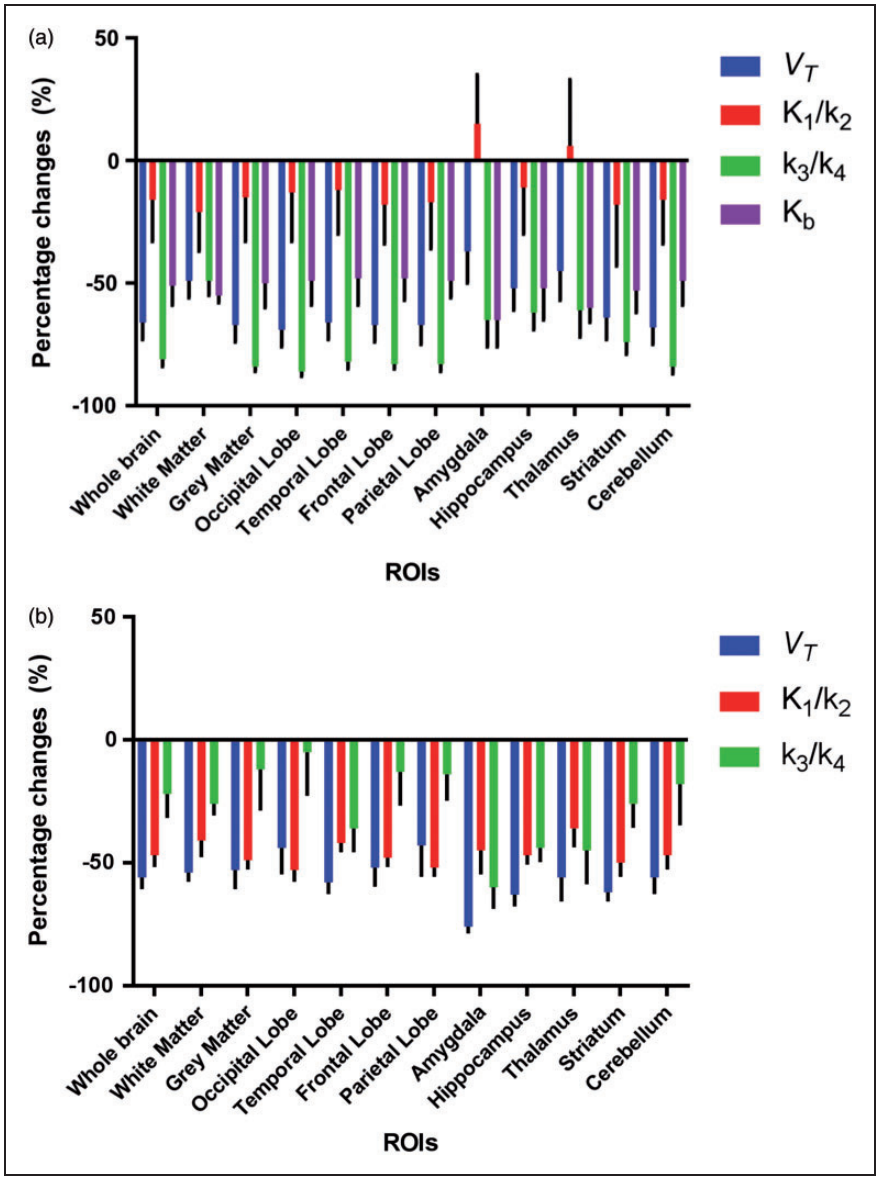

Figure 4. Effect of XBD173 on [^{11}C]PBR28brain PET kinetic estimates. Percentage changes of model kinetic parameter estimates between baseline and XBD173 blockage for 2TCM-1K (a) and standard 2TCM (b). Mean $\pm$ SD across seven subjects with schizophrenia are reported in several ROIs. Blue bars indicate V_T changes. Red bars indicate non-displaceable compartment changes (measured as K_1/k_2). Green bars indicate specific binding changes (measured as k_3/k_4). Purple bars indicate K_b changes.

variations were detected for V_T estimates (V_T mrd%: −76%:−43%), followed by the non-displaceable compartment (K_1/k_2 mrd%: −53% to −36%). The specific compartment estimates, instead, showed quite a variable behaviour (k_3/k_4 mrd%: −60% to −5%), but were still correlated with V_T changes (Pearson's r = 0.85).

Notably, while V_T variations are comparable between models (two-tailed paired t-test $p > 0.1$), K_1/k_2 and k_3/k_4 changes due to XBD173 are not (two-tailed paired t-test $p < 0.001$). These variations in the specific and nonspecific compartments for both 2TCM and 2TCM-1K are consistent with the model compartmentalisation of the total PET tracer uptake when fitting the data (Figure 3). The major differences are visible in blocking condition: while in the 2TCM-1K, the specific compartment activity becomes negligible compared to the total signal, in 2TCM, it assumes an almost irreversible kinetic in order to fit the last part of the measured data.

No difference was detected for blood volume estimates (V_b) between baseline-blocking conditions or models (V_b mean ± SD: 0.05 ± 0.01). No significant correlation was found between either injected mass or specific activity changes and the variations of any of the parameters of interest (i.e. V_T, K_1/k_2 or k_3/k_4) for both 2TCM and 2TCM-1K models. Given the absence of any significant relation with the kinetic model parameters, injected mass and specific activity effects were discarded from further analysis.

In terms of between-subject variability, 2TCM performed better compared to 2TCM-1K only for $\Delta K_1/k_2$ while returned higher CV for $\Delta k_3/k_4$. No difference was found for CV ΔV_T (p-value = 0.06). With 2TCM, inter-subject CVs were 6% for ΔV_T, 5% for $\Delta K_1/k_2$ and 11% for $\Delta k_3/k_4$. With 2TCM-1K, inter-subject CVs were 9% for ΔV_T, 20% for $\Delta K_1/k_2$, 5% for $\Delta k_3/k_4$ and 9% for ΔK_b.

Analysis of model parameter covariance showed some differences between models when compared across subjects and ROIs. Correlation between K_1/k_2 and V_T was 0.2 ± 0.1 for 2TCM and 0.7 ± 0.1 for 2TCM-1K. Correlation between k_3/k_4 and V_T was 0.6 ± 0.1 for 2TCM and 0.5 ± 0.3 for 2TCM-1K. 2TCM-1K K_b, instead, inversely correlated with all the other model parameters: −0.7 ± 0.2 with V_T, −0.6 ± 0.2 with K_1/k_2 and −0.1 ± 0.3 with k_3/k_4. Results refer to Pearson's correlation coefficient r.

Relationship between TSPO mRNA expression and kinetic estimates. With 2TCM-1K, the variations of V_T and K_b estimates due to XBD173 blockage were significantly correlated with TSPO mRNA expression (adjusted R^2: 0.84, p-value < 0.01 for V_T; 0.68, p-value < 0.01 for K_b) while 2TCM V_T changes were not (adjusted R^2: 0.15, p-value = 0.21). Comparison of the two models vs. mRNA TSPO expression is reported in supplementary material – Figure 5.

Notably, SUV variations were statistically correlated with TSPO mRNA expression but to a lesser extent compared to kinetic estimates (adjusted R^2: 0.28, p-value = 0.04).

Microscopic analysis of TSPO in vessels

We investigated the extent of TSPO expression in cortical and white matter vessel in the frontal lobe and cerebellum of three normal post-mortem brains. Immunoperoxidase immunohistochemistry analysis showed widespread TSPO expression across all brain regions and in both the grey and white matter. Small arteries, arterioles, veins and venules appeared to express higher TSPO than capillaries. As previously shown,[17] the TSPO was seen in both the endothelium and smooth muscle cells of the tunica media. Perivascular macrophages were also positive (Figure 5(a)). Double immunofluorescence confirmed the endothelial and smooth muscle cells expression of TSPO and showed that perivascular astrocytes, and their end-feed in particular were negative (Figure 5(b) and (c)).

In order to provide a more accurate estimate of vascular TSPO that could be translated into imaging studies, we used a 3D approach (Figure 6). 3D analysis of cortex and white matter of both the frontal lobe and cerebellum showed patchy TSPO expression along vessels accounting for 30% of the vascular volume in cortex and white matter. Though not prominent in the sections used for 3D analysis, perivascular macrophages could not be excluded from measurement and therefore contributed to the overall volume of vascular TSPO, which was therefore slightly overestimated. We also found that the vasculature of the cerebellar white matter was denser than the frontal lobe white matter and that TSPO expression was therefore higher (Figure 7(a) to (c) and Supplementary material – Table 5). This result was confirmed by mRNA analysis from Allen Human Brain Atlas (Figure 7(d)).

Discussion

In this study, we provided additional validation for the 2TCM-1K kinetic model for the quantification of [^{11}C]PBR28 PET data. When applied to data obtained after XBD173 administration, the 2TCM-1K produced the expected large changes in the concentration of the specific tissue compartment and vascular TSPO availability, while changes in the non-displaceable compartment were negligible. By contrast, most of the changes in concentration in the standard 2TCM were in the non-displaceable compartment indicating the unsuitability of this model to accurately describe the kinetics

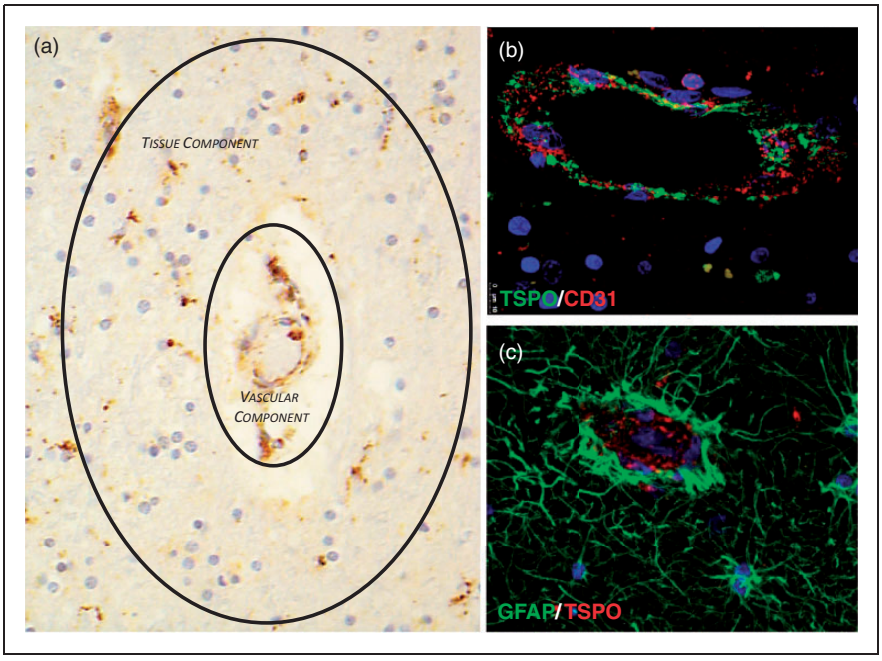

Figure 5. Expression of TSPO in a tissue section of frontal lobe – TSPO is expressed in endothelium and tunica media of cortical and white matter vessels including arteries, veins, arterioles and venuoles. TSPO is also expressed in blood mononucleated cells and perivascular macrophages. The sum of these components contributes to the vascular component of the 2TCM-1K model. At the same time, tissue microglia are also TSPO positive representing the tissue component of the both 2TCM and 2TCM-1K models (a, TSPO immunoperoxidase – ×20); confocal double immunofluorescence demonstrates TSPO expression in endothelium but the two molecule do not co-localise, the TSPO being a mitochondrial protein and CD31 (PECAM-1) an adhesion molecule on the cell surface (b, double immunofluorescence, CD31 red; TSPO green; nuclear counterstaining with DAPI, blue – ×20); perivascular reactive astrocytes and their end feed do not express TSPO (c, double immunofluorescence, TSPO red; GFAP green; nuclear counterstaining with DAPI, blue – ×20)

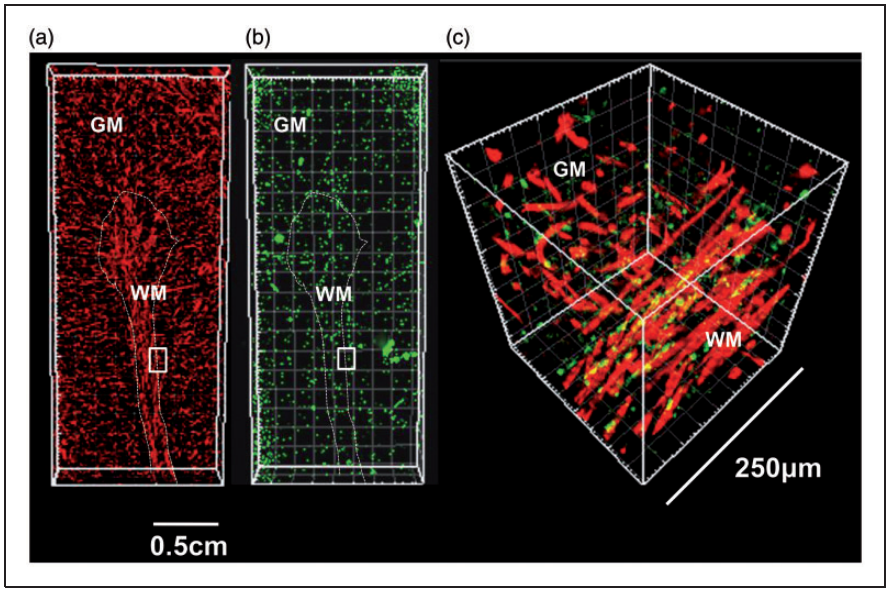

Figure 6. Vascular network and vascular TSPO in a cerebellar folium – three dimensional reconstruction of vessels and TSPO expression in a cerebellar folium using serial sections immunostained for CD31 (endothelium) and TSPO (a, CD31 red; b, TSPO green); localisation of TSPO in endothelial cells is demonstrated in a magnified 250 μm^3 volume of a region at the junction between cortex and white matter (c, CD31 red; TSPO green; co-localisation appears in yellow). The insets in images A and B indicate the region magnified in C (GM: grey matter; WM: white matter).

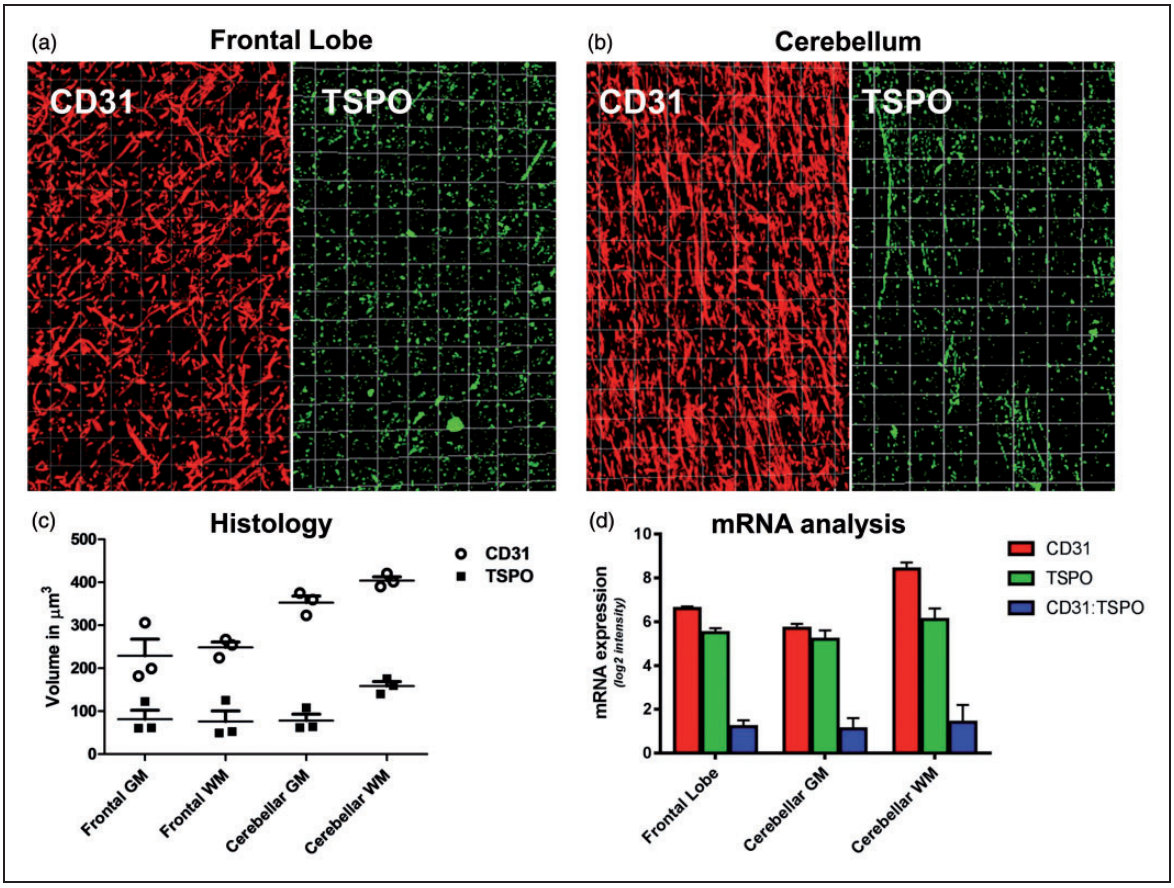

Figure 7. Variation of vascular TSPO in tissue 3D model – Three dimensional reconstruction of vessels and TSPO expression in a frontal lobe (a) and cerebellum (b) using serial sections immunostained for CD31 (endothelium) and TSPO (CD31 red; TSPO green). (c) Graphical representation of the density of the whole vascular network and TSPO positive vessels per volume units of 500 μm^3 in the cortex and white matter of frontal lobe and cerebellum; the values are calculated in three different regions of interest. (d) CD31 (red) and TSPO (green) mRNA expression as derived by Allen Human brain atlas (mean $\pm$ SD across six donors); notably, the ratio between CD31 and TSPO mRNA expression (blue) results constant across brain ROIs (mean $\pm$ SD: 1.23 $\pm$ 0.07).

induced by the reduction of TSPO density. This finding is consistent with previous applications of [^{11}C]PBR28 in healthy individuals and patients with CNS diseases,[19,21] showing that 2TCM-1K leads to a better and more efficient data description (improved fit and lower Akaike coefficient) compared to standard 2TCM. Moreover, the 2TCM-1K has also been shown to be more sensitive to changes in affinity as demonstrated by its better sensitivity to changes in rs6971 polymorphism.[19] Our results also extend previous findings that 2TCM-1K binding estimates are in better agreement with TSPO mRNA expression than those provided by 2TCM; this was demonstrated both in terms of binding data at baseline[19] and here in terms of displacement.

This study analysed [^{11}C]PBR28 binding and proposed the 2TCM-1K model in subjects with schizophrenia. Previous work by Kreczmanski et al.[34] showed no overt differences in the density of cortical capillaries between normal brains and brains with schizophrenia[34] suggesting that results obtained in this study can be extended to normal subjects. Moreover, although these results were obtained with [^{11}C]PBR28, we expect the 2TCM-1K to be applicable to other second-generation TSPO tracers. A similar data description to that provided by 2TCM-1K for [^{11}C]PBR28 brain PET data has already been reported in literature for [^{11}C]PK11195 using spectral analysis (see Figure 5 in Turkheimer et al.[17]), while preliminary results with [^{18}F]DPA-714 PET highlight the need to account for the vascular binding when fitting the data.[35]

In order to further investigate the assumption of a vascular binding component in the 2TCM-1K model, we performed immunohistochemistry for the endothelial adhesion molecule PECAM-1 (CD31) and TSPO. Results confirmed previous studies showing TSPO expression in the endothelium and tunica media of leptomeningeal, cortical and white matter vessels.[36,37]

Saturation binding studies and immunohistochemical studies have confirmed it in different conditions.[38–41] No data are available on expression in pericytes. In the brain, the vessels are surrounded by astrocytic end feet, which are tightly attached to the wall. Double immunofluorescence experiments in our study did not demonstrate any TSPO in perivascular astrocytes.

Quantification of PET signal is based on 3D evaluation (voxel), while immunohistochemistry on tissue sections gives a bi-dimensional (pixel) of TSPO localisation. To further validate PET imaging data, we built 3D immunohistochemistry images of cortical and white matter vessels, (volume comparable to imaging voxels) and quantified TSPO expression related to the volume of vessels as a surrogate measure of vascular TSPO density. TSPO expression was discontinuous but present in all vessels and accounting for 30% of the vascular network. This result is agreement with preclinical findings showing that TSPO expression in endothelial cells is comparable with the one of microglia (Supplementary Material – Figure 6).[42] Our data also showed that the ratio of TSPO and vessel volume remains similar in the cortex and grey matter but the absolute expression of vascular TSPO in the cerebellar white matter appeared higher than the other regions due to the higher vessel density per volume unit. These results were confirmed by [^{11}C]PBR28 PET data analysis: compared to cerebellar grey matter, 2TCM-1K endothelial binding statistically increased (mean $\pm$ SD across subjects: $7\% \pm 6\%$) when cerebellar white matter was included in the analysis (two-tailed paired t-test p-value < 0.01). It follows that TSPO PET data analysis of cerebellum needs to account for its complex cellular heterogeneity. This characteristic together with the observed high TSPO displacement does not make the cerebellum an ideal reference region for TSPO PET imaging studies.

The adult brain microvasculature has an overall surface area of about $100\,cm^2/g$ tissue with an overall volume of capillaries accounting for about $200\,cm^3$ of an average total brain volume of $1200\,cm^3$.[43] With such density of blood vessels, and such high endothelial TSPO expression, the widespread vascular TSPO documented in our study explains the diffuse rather than discrete signal of vascular TSPO, which is high in the cortex and it is often interpreted as the result of non-specific binding. It is worth remembering that vascular supply in the normal brain is not uniform across regions and that changes occur in ageing and pathological conditions. There is evidence of a reduction of vessel density in aging with an overall average decrease of 16% in capillary density and a decline in the density of white matter vessels between the fifth and ninth decades. Mann et al.[44] found a decrease in vessel density in frontal cortex, but not in the temporal cortex. In addition, small vessel disease including hyalinization of the wall with loss of smooth muscle cells also impacts on TSPO expression. Robust and reproducible modelling of vascular TSPO is therefore relevant to the interpretation of data from normal subjects and patients with brain diseases.

The evidence provided in our study supports the 2TCM-1K compartmentalization. Beyond the relevance for PET quantification, the pharmacokinetics of these compartments indicates that the targeting of TSPO in microglia is not a trivial task as a significant percentage of TSPO compounds will bind to the vessels and produce an unknown/unwanted modulatory effects on the BBB. To this extent, it is important to note that using endothelial cells derived from human umbilical vein,[38] documented TSPO upregulation following stimulation with TNF. Overexpression of TSPO in adenovirus transfected cells resulted in protection against TNF-induced endothelial activation including inhibition of VCAM-1 and ICAM-1 expression, resulting in reduced monocyte adhesion, inhibition of ROS production, decrease of mitochondrial manganese superoxide dismutase and downregulation of the Voltage Dependent Anion Channel-1.[38] In contrast, these results suggest that a reduction of TSPO may increase the permeability of the BBB and trafficking of inflammatory cells.

The dynamics we observed in the blood following XBD173 modulation were also of interest. Quantification of PET ligands using arterial input function is regarded as the best quantitative measure but it is based on the assumption that the parent plasma concentration of the tracer is correct. In this study, we observed variable kinetic in the various TSPO blood compartments. Owen et al.[9] proposed the use of blocking studies, like XBD173, to confirm whether V_T global changes are driven by TSPO-specific signal changes. Our results do not support the use of this methodology as the administration of TSPO blocking agents such as XBD173 has a significant impact on [^{11}C]PBR28 binding in blood itself and seems to alter the plasma free fractions therefore reducing, and not improving, the accuracy of the brain measures.

One key aspect of the complexity of [^{11}C]PBR28 kinetics is the apparent difference between the reversible binding profile of the tracer to the parenchima and the irreversible binding to the endothelium. Previously, we explained this difference in terms of varying reactive volumes, which means that while it is the free plasma concentration of the tracer that exchanges with endothelial TSPO, only the free fraction in tissue reaches the mitochondria exchanges with TSPO in microglia and astrocytes. This is not properly modelled by the one only compartment of the 2TCM model where the free tracer concentration in reality is the average of a likely

steep gradient of concentration, decreasing from the blood–brain barrier to the intracellular space and mitochondria.[45] Please note that the affinity for TSPO of PBR28 is very high, 4 nmol/L[8] which then translates in the 90 min of the experimental time into apparent irreversibility. Moreover, modelling the endothelial tracer binding with a reversible exchange together with a two-tissue compartmental model description does not guarantee the model parameter identifiability (Supplementary material – "Study of a priori identifiability of 2TCM-2K model").

Limitations

This work presents some limitations. The blocking studies were performed two years after the baseline for six out of seven patients of the dataset. The presence of disease as well as the well-known interaction between treatment and TSPO density[46] do not allow to assume that the level of inflammations remained the same between the two scans. One should, however note, that inflammation in these cohorts resulted in <10% TSPO density increase on average;[21,47] hence, we did not expect that any change in TSPO due to modulation of inflammation by disease or treatment would alter substantially the displacement of TSPO that in overall was greater than 50%.

In this experimental design, only one structural MRI scan at baseline was performed. The procedure might be suboptimal due to the presence of brain changes over time that are expected patients with schizophrenia[48] as well as in healthy adults.[49] However, we expect minimum impact of structural changes on our results, as the MRI was only used to assist with atlas coregistration to PET images, and our analysis was limited to large regions of interest.

The use of microparameter ratios (i.e. K_1/k_2 and k_3/k_4) as proxy of the nondisplaceable distribution volume and tracer binding potential is penalised by higher sensitivity to noise compared to V_T estimates. However, the ratios K_1/k_2 and k_3/k_4 are not used as group metrics in a cross-sectional design but only as metrics of performance for competing kinetic models; here, the expected reduced availability of TSPO due to drug occupancy should be translated into changes of the specific bound compartment. From a theoretical perspective, K_1/k_2 ratio should be constant throughout the brain ROIs in both baseline and blocking studies; since the aim of the study was the investigation of the compartmental structure for this tracer, this ratio was not fixed during the optimization and we did notice significant variability across brain. To note that microparameters have general validity in quantification.[50,51] Importantly, microparameters and compartmental models are the key to make predictions and guide tracer development and this has been particularly the case for TSPO ligands, where previous synthetic work using the standard 2TCM model has not been supported by data in-vivo.[52] In general terms, the kinetic components in compartmental modelling are not orthogonal (by definition as the exponential base is not orthogonal), hence substantial covariance across microparameters is expected. In the case of the 2TCM1K, K_b is inversely correlated with all the parenchyma components (V_T, K_1/k_2 and k_3/k_4) as they are biologically contrasted; the more tracer is associated to vascular binding the less is available to the tissue for both specific and non-displaceable binding.

The use of TSPO mRNA as proxy of TSPO protein density also needs to be critically considered: mRNA is an indicator of gene regulation but not necessarily of protein expression.[31] Moreover, TSPO mRNA expressions from Allen Brain Atlas do not distinguish the cellular source of TSPO (glial or vascular). However, we found good correlation between kinetic parameter changes following XBD173 administration and TSPO mRNA, despite the fact that the imaging dataset refers to patients with schizophrenia, while the mRNA atlas to healthy controls. TSPO density increased in SCHZ patients have shown to be limited;[21,47] hence, the changes observed were mostly due to TSPO density unrelated to the disorder.

Conclusions

In conclusion, we demonstrated that the accounting for endothelial TSPO gives a more precise and accurate quantification of [^{11}C]PBR28 brain PET data that are consistent with TSPO biology. TSPO expression in vessels using 3D reconstructions of histological data of frontal lobe and cerebellum demonstrates that TSPO positive vessels account for 30% of the vascular volume in cortical and white matter.

Funding

The author(s) disclosed receipt of the following financial support for the research, authorship, and/or publication of this article: MV and FET are supported by the Wellcome Trust "Strategic Award: Inflammation in AD and MDD". MV is also supported by the National Institute for Health Research (NIHR) Biomedical Research Centre at South London and Maudsley NHS Foundation Trust and King's College London. FR and DM work leading to these results has received funding from the European Union's Seventh Framework Programme (FP7/2007-2013) under grant agreement n° HEALTH-F2-2011-278850 (INMiND) and MRC Research Grant" Pathfinder: An experimental medicine study of the 18 kD translocator protein as a novel neuroimmunodulatory target for multiple sclerosis" No MR/N026934/1. Tissue (or cerebrospinal fluid) samples and

associated clinical and neuropathological data were supplied by the Parkinson's UK Brain Bank, funded by Parkinson's UK, a charity registered in England and Wales (258197) and in Scotland (SC037554).

Acknowledgments

We thank the UK Parkinson's Tissue Bank at Imperial College for supplying the samples of normal brain tissue and donors and their families for making this project possible. We are grateful to Dr Peter March of the Bioimaging Centre at the University of Manchester, UK (www.ls.manchester.ac.uk) for guidance in 3D tissue modelling. Mrs Helen Mayers at the Department of Cellular Pathology, Salford Royal Foundation Hospital, Salford UK, is thanked for immunohistochemistry for TSPO and CD31.

Declaration of conflicting interests

The author(s) declared the following potential conflicts of interest with respect to the research, authorship, and/or publication of this article: The authors declare that the research was conducted in the absence of any commercial or financial relationships that could be construed as a potential conflict of interest. Federico Turkheimer reports receiving lecture fees from Eli-Lilly.

Authors' contributions

MV, TM, OH, FR and FET made substantial contribution to the study design. MV, TM, PSB, GR, DJ, EA, DM, OH, FR and FET made substantial contribution to the data collection and analysis. MV, TM, PSB, GR, NS, AB, OH, FR and FET made substantial contribution to the data interpretation. MV, PSB, GR, AB, OH, FR and FET drafted the manuscript. All the authors critically revised the article. All authors approved the last version.

Supplementary material

Supplementary material for this paper can be found at the journal website: http://journals.sagepub.com/home/jcb

References

1. Gatliff J and Campanella M. The 18 kDa Translocator protein (TSPO): a new perspective in mitochondrial biology. *Curr Mol Med* 2012; 12: 356–368.
2. Chen M-K and Guilarte TR. Translocator protein 18 kDa (TSPO): molecular sensor of brain injury and repair. *Pharmacol Ther* 2008; 118: 1–17.
3. Rupprecht R, Papadopoulos V, Rammes G, et al. Translocator protein (18 kDa)(TSPO) as a therapeutic target for neurological and psychiatric disorders. *Nat Rev Drug Discov* 2010; 9: 971–988.
4. Vivash LE and O'Brien TJ. Imaging microglial activation with TSPO PET: lighting up:neurological diseases? *J Nucl Med* 2015; 57: 165–168.
5. Venneti S, Lopresti BJ and Wiley CA. The peripheral benzodiazepine receptor (Translocator protein 18kDa) in microglia: from pathology to imaging. *Progr Neurobiol* 2006; 80: 308–322.
6. Hinz R and Boellaard R. Challenges of quantification of TSPO in the human brain. *Clin Transl Imag* 2015; 3: 403–416.
7. Turkheimer FE, Rizzo G, Bloomfield PS, et al. The methodology of TSPO imaging with positron emission tomography. *Biochem Soc Transac* 2015; 43: 586–592.
8. Owen DR, Yeo AJ, Gunn RN, et al. An 18-kDa translocator protein (TSPO) polymorphism explains differences in binding affinity of the PET radioligand PBR28. *J Cereb Blood Flow Metab* 2012; 32: 1–5.
9. Owen D, Guo Q, Rabiner E, et al. The impact of the rs6971 polymorphism in TSPO for quantification and study design. *Clin Transl Imag* 2015; 3: 417–422.
10. Martini C, Chelli B, Betti L, et al. Peripheral benzodiazepine binding sites in platelets of patients affected by mitochondrial diseases and large scale mitochondrial DNA rearrangements. *Mol Med* 2002; 8: 841.
11. Soreni N, Apter A, Weizman A, et al. Decreased platelet peripheral-type benzodiazepine receptors in adolescent inpatients with repeated suicide attempts. *Biol Psychiatr* 1999; 46: 484–488.
12. Pini S, Martini C, Abelli M, et al. Peripheral-type benzodiazepine receptor binding sites in platelets of patients with panic disorder associated to separation anxiety symptoms. *Psychopharmacology* 2005; 181: 407–411.
13. Begni B, Tremolizzo L, Andreoni S, et al. Neuroligand binding endophenotypes in blood cells distinguish two subsets of borderline personality disorder patients. *Neurosci Lett* 2009; 462: 144–146.
14. Ritsner M, Modai I, Gibel A, et al. Decreased platelet peripheral-type benzodiazepine receptors in persistently violent schizophrenia patients. *J Psychiatr Res* 2003; 37: 549–556.
15. Lockhart A, Davis B, Matthews JC, et al. The peripheral benzodiazepine receptor ligand PK11195 binds with high affinity to the acute phase reactant α1-acid glycoprotein: implications for the use of the ligand as a CNS inflammatory marker. *Nucl Med Biol* 2003; 30: 199–206.
16. Albrecht DS, Granziera C, Hooker JM, et al. In vivo imaging of human neuroinflammation. *ACS Chem Neurosci* 2016; 7: 470–483.
17. Turkheimer FE, Edison P, Pavese N, et al. Reference and target region modeling of [11C]-(R)-PK11195 brain studies. *J Nucl Med* 2007; 48: 158–167.
18. Tomasi G, Edison P, Bertoldo A, et al. Novel reference region model reveals increased microglial and reduced vascular binding of 11C-(R)-PK11195 in patients with Alzheimer's disease. *J Nucl Med* 2008; 49: 1249–1256.
19. Rizzo G, Veronese M, Tonietto M, et al. Kinetic modeling without accounting for the vascular component impairs the quantification of [11C] PBR28 brain PET data. *J Cereb Blood Flow Metab* 2014; 34: 1060–1069.
20. Brown AK, Fujita M, Fujimura Y, et al. Radiation dosimetry and biodistribution in monkey and man of 11C-PBR28: a PET radioligand to image inflammation. *J Nucl Med* 2007; 48: 2072–2079.
21. Bloomfield PS, Selvaraj S, Veronese M, et al. Microglial activity in people at ultra high risk of psychosis and in

schizophrenia: an [11C] PBR28 PET brain imaging study. *Am J Psychiatr* 2016; 173: 44–52.
22. Collste K, Forsberg A, Varrone A, et al. Test–retest reproducibility of [11C] PBR28 binding to TSPO in healthy control subjects. *Eur J Nucl Med Mol Imag* 2016; 43: 173–183.
23. Coughlin JM, Wang Y, Ma S, et al. Regional brain distribution of translocator protein using [11C] DPA-713 PET in individuals infected with HIV. *J Neurovirol* 2014; 20: 219–232.
24. Owen DR, Guo Q, Kalk NJ, et al. Determination of [(11) C] PBR28 binding potential in vivo: a first human TSPO blocking study. *J Cereb Blood Flow Metab* 2014; 34: 1256.
25. Edison P, Brooks DJ, Turkheimer FE, et al. Strategies for the generation of parametric images of [11C]PIB with plasma input functions considering discriminations and reproducibility. *Neuroimage* 2009; 48: 329–338.
26. Tonietto M, Veronese M, Rizzo G, et al. Improved models for plasma radiometabolite correction and their impact on kinetic quantification in PET studies. *J Cereb Blood Flow Metab* 2015; 35: 1462–1469.
27. Modelling arterial input functions in positron emission tomography dynamic studies. In: *37th Annual International Conference of the IEEE on Engineering in Medicine and Biology Society (EMBC)*, Milan, Italy, 25–29 August 2015, pp. 2247–2250.
28. Bertoldo A, Vicini P, Sambuceti G, et al. Evaluation of compartmental and spectral analysis models of [/sup 18/ F] FDG kinetics for heart and brain studies with PET. *IEEE Trans Biomed Eng* 1998; 45: 1429–1448.
29. Akaike H. A new look at the statistical model identification. *IEEE Trans Automat Control* 1974; 19: 716–723.
30. Hawrylycz MJ, Lein S, Guillozet-Bongaarts AL, et al. An anatomically comprehensive atlas of the adult human brain transcriptome. *Nature* 2012; 489: 391–399.
31. Rizzo G, Veronese M, Heckemann RA, et al. The predictive power of brain mRNA mappings for in vivo protein density: a positron emission tomography correlation study. *J Cereb Blood Flow Metab* 2014; 34: 827–835.
32. Rizzo G, Veronese M, Expert P, et al. MENGA: A new comprehensive tool for the integration of neuroimaging data and the Allen human brain transcriptome atlas. *PloS One* 2016; 11: e0148744.
33. Cassoni P, Gaetano L, Senetta R, et al. Histology far away from Flatland: 3D roller-coasting into grade-dependent angiogenetic patterns in oligodendrogliomas. *J Cell Mol Med* 2008; 12: 564–568.
34. Kreczmanski P, Heinsen H, Mantua V, et al. Volume, neuron density and total neuron number in five subcortical regions in schizophrenia. *Brain* 2007; 130: 678–692.
35. Wimberley C, Stute S, Lavisse S, et al. Optimisation of quantification for 18F-DPA-714 in the healthy human. *J Nucl Med* 2016; 57(supplement 2): 95.
36. Gavish M, Bachman I, Shoukrun R, et al. Enigma of the peripheral benzodiazepine receptor. *Pharmacol Rev* 1999; 51: 629–650.
37. Papadopoulos V. Peripheral-type benzodiazepine/diazepam binding inhibitor receptor: biological role in steroidogenic cell function. *Endoc Rev* 1993; 14: 222–240.
38. Joo HK, Lee YR, Lim SY, et al. Peripheral benzodiazepine receptor regulates vascular endothelial activations via suppression of the voltage-dependent anion channel-1. *FEBS Lett* 2012; 586: 1349–1355.
39. Veenman L and Gavish M. The peripheral-type benzodiazepine receptor and the cardiovascular system. Implications for drug development. *Pharmacol Ther* 2006; 110: 503–524.
40. Cosenza-Nashat M, Zhao ML, et al. Expression of the translocator protein of 18 kDa by microglia, macrophages and astrocytes based on immunohistochemical localization in abnormal human brain. *Neuropath Appl Neurobiol* 2009; 35: 306–328.
41. Bird J, Izquierdo-Garcia D, Davies J, et al. Evaluation of translocator protein quantification as a tool for characterising macrophage burden in human carotid atherosclerosis. *Atherosclerosis* 2010; 210: 388–391.
42. Zhang Y, Chen K, Sloan SA, et al. An RNA-sequencing transcriptome and splicing database of glia, neurons, and vascular cells of the cerebral cortex. *J Neurosci* 2014; 34: 11929–11947.
43. Pardridge WM, Triguero D, Yang J, et al. Comparison of in vitro and in vivo models of drug transcytosis through the blood-brain barrier. *J Pharmacol Exp Ther* 1990; 253: 884–891.
44. Mann DM, Eaves NR, Marcyniuk B, et al. Quantitative changes in cerebral cortical microvasculature in ageing and dementia. *Neurobiol Aging* 1986; 7: 321–330.
45. Delforge J, Syrota A and Bendriem B. Concept of reaction volume in the in vivo ligand-receptor model. *J Nucl Med* 1996; 37: 118–125.
46. Cotel M-C, Lenartowicz EM, Natesan S, et al. Microglial activation in the rat brain following chronic antipsychotic treatment at clinically relevant doses. *Eur Neuropsychopharmacol* 2015; 25: 2098–2107.
47. van Berckel BN, Bossong MG, Boellaard R, et al. Microglia activation in recent-onset schizophrenia: a quantitative (R)-[11 C] PK11195 positron emission tomography study. *Biol Psychiatr* 2008; 64: 820–822.
48. Wright IC, Rabe-Hesketh S, Woodruff PW, et al. Meta-analysis of regional brain volumes in schizophrenia. *Am J Psychiatr* 2000; 157: 16–25.
49. Raz N, Lindenberger U, Rodrigue KM, et al. Regional brain changes in aging healthy adults: general trends, individual differences and modifiers. *Cereb Cortex* 2005; 15: 1676–1689.
50. Cunningham VJ, Rabiner EA, Matthews JC, et al. Kinetic analysis of neuroreceptor binding using PET. *Int Cong Ser* 2004; 1265: 12–24.
51. Slifstein M, van de Giessen E, Van Snellenberg J, et al. Deficits in prefrontal cortical and extrastriatal dopamine release in schizophrenia: a positron emission tomographic functional magnetic resonance imaging study. *JAMA Psychiatr* 2015; 72: 316–324.
52. Guo Q, Owen DR, Rabiner EA, et al. Identifying improved TSPO PET imaging probes through biomathematics: the impact of multiple TSPO binding sites in vivo. *Neuroimage* 2012; 60: 902–910.